

Recent progress on micro- and nano-robots: towards *in vivo* tracking and localization

Ben Wang^{1,2#}, Yabin Zhang^{1,2#}, Li Zhang^{1,3,4}

¹Department of Mechanical and Automation Engineering, ²Department of Biomedical Engineering, ³Chow Yuk Ho Technology Centre for Innovative Medicine, ⁴T Stone Robotics Institute, The Chinese University of Hong Kong, Hong Kong, China

#These authors contributed equally to this work.

Correspondence to: Li Zhang. Department of Mechanical and Automation Engineering, The Chinese University of Hong Kong, Hong Kong, China. Email: lizhang@mae.cuhk.edu.hk.

Submitted Jun 01, 2018. Accepted for publication Jun 18, 2018.

doi: 10.21037/qims.2018.06.07

View this article at: <http://dx.doi.org/10.21037/qims.2018.06.07>

Introduction

Scientists have dreamed for long of miniature robots that can be controlled and navigated inside human body, to help the medical doctors to diagnose and treat the diseases. As shown by the old classic movie *Fantastic Voyage* released in 1966, a submarine with a group of crews was shrunk to the micro-scale so that it can navigate inside the human blood vessel for the removal of a blood clot. To explore the possibility to realize that wild idea, scientists have proposed and developed many types of miniature machines and robots, some of which are aimed to adapt various kinds of physiological environments for diagnosis and disease treatment. A variety of micro- and nano-scale robots have been developed among the past decade, which offer promise for diverse biomedical applications (1-14). The key factors for constructing the biomedical micro- and nano-scale robots are the controllability, visuality, functionality and biocompatibility. Apart from the macroscale robots, the micro- and nano-scale robots applied in the fluid environments may face to significant difficulties in motion due to the low Reynolds number. To actuate and steer the tiny robots in the low Reynolds number regime where inertia is negligible compared to the viscous force, special strategies for locomotion should be developed. Basically, the micro-/nanorobots can be classified into natural/biological, artificial and biohybrid types, and the artificial micro-/nanoagents are often divided into self-propelled, and external field propelled ones, according to the type of input

energy (15). The self-propelled micro-/nano-robots usually generate continuous propulsion from the environment in the form of self-electrophoresis, self-thermophoresis, self-diffusiophoresis and tiny bubbles. In contrast, the external field propelled micro-/nanorobots can be actuated only if the external field, such as magnetic field, electric field, light, US waves and so on, is applied.

In order to facilitate the biomedical applications of the micro-/nanorobots, in particular for *in vivo* applications, imaging and real-time tracking of these tiny agents are crucial. To date, a variety of imaging techniques, including fluorescent imaging (FI), magnetic resonance imaging (MRI), ultrasonic (US) imaging, computed tomography (CT), positron emission tomography (PET) and single-photon emission computed tomography (SPECT) have been explored for localization of micro- and nano-scale robots, as shown in *Figure 1*. Benefiting from the synergy of imaging and motion, the resultant micro-/nano-scale robots can be not only tracked in real time *in vitro* and even *in vivo*, but also used to realize targeted delivery/therapy in a destined location with vision-based control. Moreover, the introduction of the additional motion of the micro-/nano-agents may also enhance the imaging contrast due to the dynamics compared with the static micro-/nano-agents. Built on the great progress on the nano-/micro-particles and active matters in biomedical imaging (20,21), the mobile micro- and nano-robots imaging techniques may offer a brand-new active tool for targeting specific sites and accomplishing

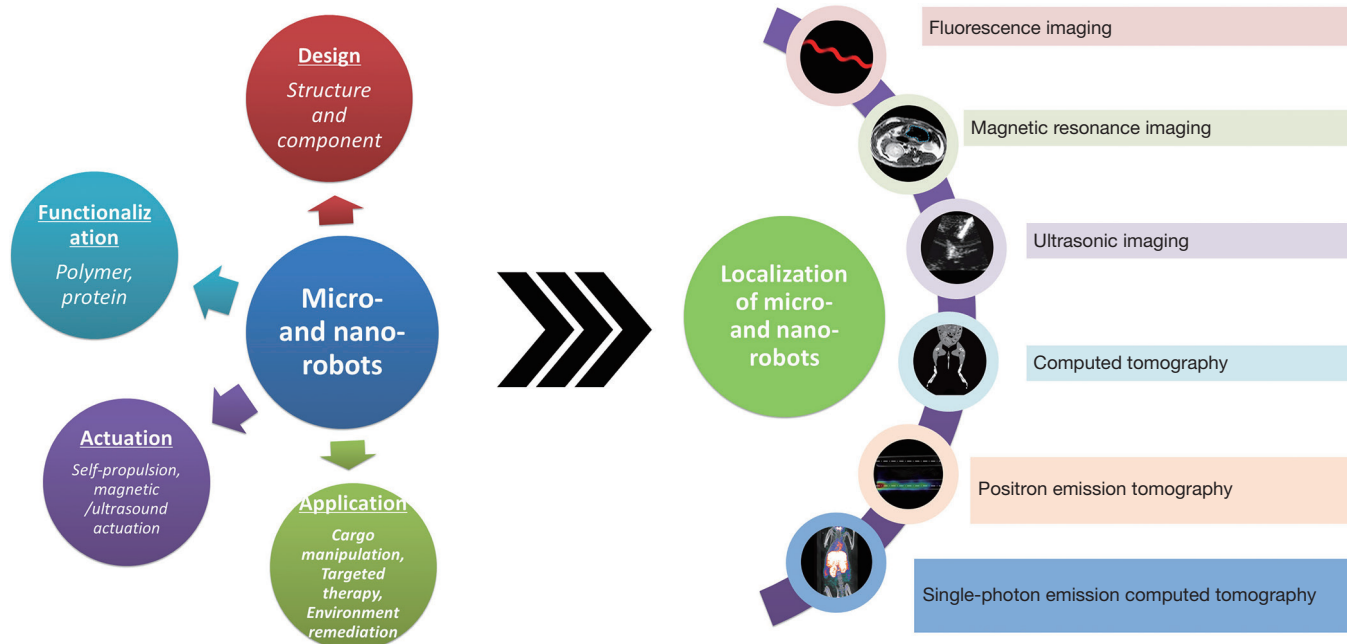


Figure 1 Schematic illustration of the imaging techniques of micro- and nano-robots. The insets are reprinted with permission from Copyright 2017 AAAS (16), Copyright 2017 RSC (17), Copyright 2014 SAGE (18), Copyright 2018 ACS (19).

certain medical tasks in a minimally invasive fashion.

In this article, we discuss and summarize the recent progress in the development of micro- and nanorobots towards the application *in vivo*, by focusing on four kinds of bio-imaging modes, i.e., FI, radionuclide imaging (RI), MRI, and US imaging which are reported recently. And the current challenges together with future research orientation related to localization of micro-/nano-robots *in vivo* are discussed.

Imaging modalities with micro and nanorobots

Fluorescent imaging

Fluorescent technique, as a powerful *ex vivo* or *in vitro* tool for biology and biomedicine, has been widely used in biological research during the past decades for the usual examination of histological tissue samples or living cells (22,23). Compared to other highly sensitive imaging techniques, fluorescence-based technique has the advantages of the use of visible light illumination without causing harmful ionizing effects to organisms and the low cost of probe materials (24,25). On one hand, numerous fluorescent probes including organic dyes, fluorescent metal nanoclusters, semiconductor quantum dots, and fluorescent

metal organic frameworks are designed to generally label various types of cells and organelles, or even to index the presence of peculiar biomolecules (26-29). On the other hand, significant advances have been made in miniaturizing the FI to the level for catheterization or endoscopy, which can be inserted into the body with minimal invasiveness (7). Inspired by these fascinating merits and advances, the integration of this technique into micro-/nanorobots not only simplifies the tracking and targeting of micro-/nano-robotics, but also greatly extends their application to active bioimaging and bio-diagnosis. To date, various fluorescent micro-/nano-robots have been prepared through introducing the fluorescent substances, mainly including the use of intrinsically fluorescent raw materials to fabricate the robots or the incorporation of existing fluorescent labeling or tags during the preparation process. These micro-/nanorobots can achieve more precise targeting imaging under the guidance of an external field than conventional diffusion-based chemical targeting, accompanied by other advantages from active motion. Based on the difference in fluorescent modifiers, we will discuss the fluorescent micro-/nanorobots from the following aspects.

To our knowledge, various biological organisms in nature show an intrinsic fluorescence, named autofluorescence,

in the range from UV-visible light to near-IR light when excited with light at suitable wavelength (30). This widespread phenomenon is originated from the common presence of intrinsic molecules acting as endogenous fluorophores in the organisms (31). Such many endogenous fluorophores greatly influence their autofluorescence emission features, thus offer a powerful tool for the directly monitoring of the biological substrates. On the one hand, autofluorescence phenomena have a great adverse effect on the FI with other probes, especially for UV light and blue light illumination (32). On the other hand, strong and long-wavelength autofluorescence can characterize subtle changes of interconnected morphological and metabolic properties of cells and even tissues in real time under physiological conditions (33). Since the micro-/nano-robots are usually prepared using various raw materials, when some materials with the intrinsic autofluorescence are used, those devices can be endowed with fluorescence, making them show great promises in real-time tracking and localization by using the fluorescence signal.

At present, several types of micro-/nano-robots have been fabricated using autofluorescence materials for tracking their movements. The initial micro-/nano-robots were prepared by conventional photolithograph. The fluorescent elements can be easily incorporated into micro-/nano-robots due to the utilization of the organic molecules with the intrinsic fluorescence (34). SU8, as a most common material for microfabrication, shows a fluorescent emission near the blue and green region of the light spectrum, which appears as an emission agent against a black background in the captured image (35). Steager *et al.* developed a single-step fabrication process for biocompatible magnetic microrobots using composite photoresist mixed with iron oxide powder on glass slides (*Figure 2A,B*) (36). The resultant autofluorescence microrobots were used to evaluate the self-developed magnetically actuated robotic system (*Figure 2C*). Owing to autofluorescence of SU8, microrobots were visible in both blue and green emission region (*Figure 2D*). The captured fluorescent image of microrobots was entirely different from the transmitted light image, as shown in *Figure 2C,D*. By choosing an appropriate combination of fluorescent tags and filters to forming a difference between the targets and the microrobots, a novel tracking algorithm was developed for tracking fluorescent microrobots to targeting cells independently (*Figure 2E*). In this regard, these results make the fluorescent microrobots better tracked under dark field. Meanwhile, the studies also suggest that autofluorescence

phenomenon has great potential for real-time tracking of the swimming microrobots. Afterwards, inspired by nature micro-algae, Yan *et al.* reported biohybrid helical magnetic robots from *Spirulina* via a facile dip-coating process in magnetite (Fe_3O_4) suspensions (*Figure 2F*) (16). The resultant helical microrobots were superparamagnetic via an engineered coating and were endowed with desired structure and fluorescence inherited from a biological matrix. Strong red-light emission of the microrobots could be easily observed upon green light illumination without the addition of any fluorescent markers (*Figure 2G*). Thanks to an innate autofluorescence of the microalgae, the helical microrobots can be directly used *in vivo* for real-time tracking and diagnostic sensing. The corresponding imaging was demonstrated in the subcutaneous tissue and the intraperitoneal cavity of nude mice (*Figure 2H,I,J*). The image sequences of the microrobots with varied concentrations and residence time in the subcutaneous tissue were given in *Figure 2H,I,J*, showing that the fluorescence intensity increased with the sample concentration while decreased with the residence time. These results validate that the microrobots can be tracked in real time and have potentials for image guided therapy by magnetic actuation.

Although autofluorescence imaging is convenient and valuable for *in vivo* imaging application owing to its easy-to-operate specificity, some other factors constrain its biomedical applications as well. It has been demonstrated that there is a ubiquitous autofluorescence found in the major internal organs and bodily fluids due to the presence of fluorescent biomolecules such as NAD(P)H, chlorophyll, porphyrins, and collagens, which may impact the practical *in vivo* application (37,38). Furthermore, the most of the autofluorescence emissions show the common blue or green emission. Such a short-wavelength emission light is difficult to penetrate the deep tissue, hence usually only for superficial region observation (39-41). More importantly, under the same excitation light, the different autofluorescence from the microrobots and biological tissues may be emitted, which will cause a great interference for *in vivo* imaging. These limitations make the autofluorescence microrobots to some extent hindered for the clinical applications, especially in deep tissue.

Organic dyes or fluorophores has been studied for about 150 years since their discovery. During the past times, a great number of fluorescent dyes have been synthesized and applied in imaging of biomolecules, cells, and organisms (42). They have become the most common imaging contrast agents in biomedical application due to the outstanding

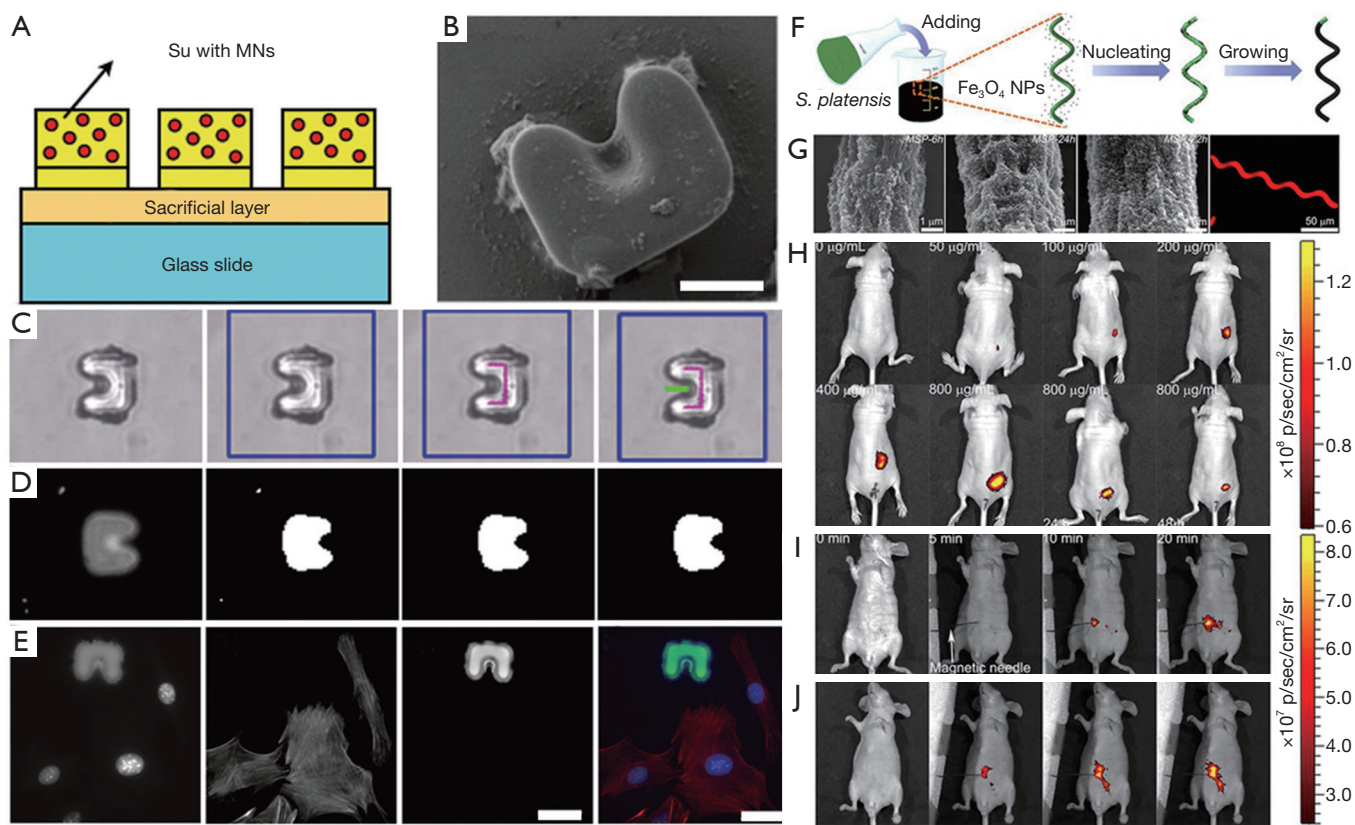


Figure 2 Autofluorescence materials based microrobots. (A) The preparation process of SU8 ferromagnetic microrobots. (B) SEM image of a single U-shaped ferromagnetic microrobot. Scale bar is 15 μm . (C,D) Time-lapse images show magnetically driven ferromagnetic microrobots under bright optical field and dark fluorescent field, respectively. (E) Real-time imaging of magnetic microrobot to target cells under fluorescence microscopy. Blue region shows the nucleus and red region shows the actin filaments inside the cell. The scale bars are 30 μm (36). (F) Schematic shows the fabrication process of *S. platensis* coated with Fe_3O_4 NPs. (G) SEM and fluorescence images of magnetic microrobots subjected to different time of dip-coating process (The fluorescence image was obtained with excitation at 552 nm). *In vivo* fluorescence imaging of magnetic microrobots: (H) using 100 μL of MSP-72 h with varied concentrations in the subcutaneous tissue of nude Balb/c athymic mice at three residence times. Using 300 μL of (I) MSP-72 h and (J) MSP-24h (all 800 g/mL) in the intraperitoneal cavity at various residence times (16). Reprinted with permission from Copyright 2013 SAGE (36), and Copyright 2017 AAAS (16). MN, magnetic nanoparticles; SEM, scanning electron microscope.

advantages, including the commercial availability of a toolbox of functionalized dyes, established labeling protocols, purification and characterization techniques for dye bioconjugates, as well as information on the site-specificity of the labeling procedure (43-45). Furthermore, the small size of organic dye molecules minimizes possible steric hindrance which can interfere with biomolecule function. This allows attachment of several fluorophores to a single biomolecule to maximize the fluorescence signal (46). In view of the above merits and facile conjugating ability, more and more organic dyes are incorporated into the fabrication of micro-/nano-structures, thus endowing

these structures with good fluorescent performance. More importantly, the integration of mobile micro-/nano-robots with dyes greatly solves the site-specificity problem of traditional chemical-targeting organic dyes.

In this regard, scientists initially introduced these dyes to track the movement of micro-/nano-robots under the dark field. Mhanna *et al.* prepared artificial bacterial flagella (ABF) microrobots functionalized with fluorescent calcein labeled liposome (Figure 3A,B) (47). Such microrobots can swim without significant loss of the calcein fluorescent signal (Figure 3B), suggesting the good fluorescent stability during the movement. The stable fluorescent emission

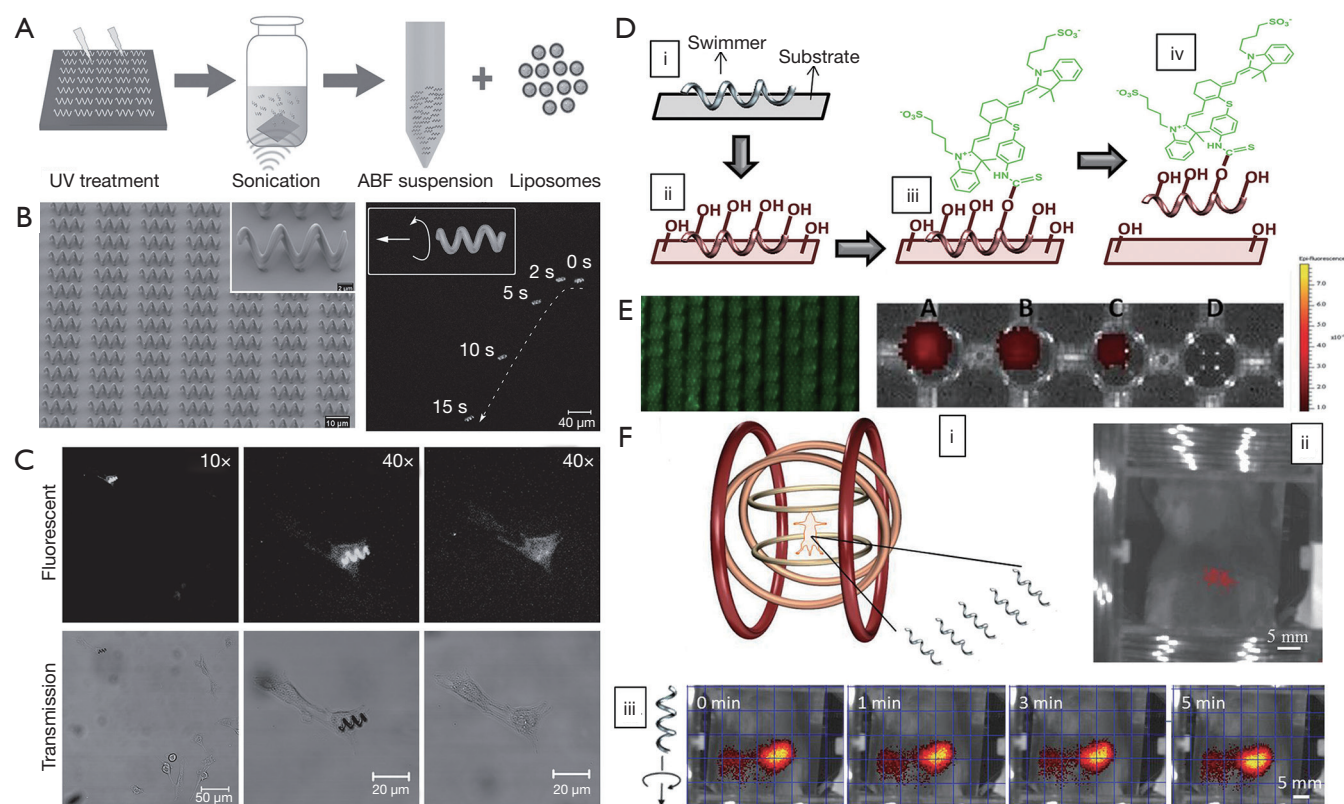


Figure 3 Dye-based microrobots. (A) Schematic shows the batch preparation of the artificial bacterial flagella (ABF) microrobots functionalized with liposome loaded with calcein. (B) SEM image of liposome-loaded ABF microrobots and fluorescent time-lapse image shows the motion under a rotating magnetic field. (C) The fluorescent and optical images show the tracking of delivery of calcein to cells by using the liposome-loaded ABF microrobots at different magnifications (47). (D) Schematic illustration of surface modification of the ABF microrobots with NIR-797 dyes. (E) The fluorescent image of the functionalized ABF microrobots and the IVIS fluorescence signal at different concentrations in IPA. (Fi) Schematic illustration of the *in vivo* experiment. (Fii) Image of an anesthetized Balb-C mouse inside the coils with 4-week-old. The red spots represent the fluorescent signal generated by the injected ABF microrobots. (Fiii) Successive images show the functionalized ABF microrobots swimming downwards. The yellow cloud was created by a homemade Matlab code and was applied to track the motion (48). Reprinted with permission from Copyright 2014 Wiley (47), Copyright 2015 Wiley (48). SEM, scanning electron microscope; IVIS, in vivo navigation system.

can be used to track the swimming and delivering process of the microrobots to cell (Figure 3C), which is also a promising candidate for the cellular imaging. However, calcein fluorescent signal is short-wavelength and is not beneficial to *in vivo* application. Servant *et al.* functionalized the ABF microrobots with near-infrared probes (NIR-797) (Figure 3D) (48). NIR-797 was selected as an emitting fluorophore because of its long wavelength emission for whole-body fluorescence imaging. The intensity of the fluorescent signal of the NIR-ABF microrobots varied in the different solvent systems, in agreement with the extinction coefficient of NIR-797 in the same solvents (Figure 3E). The fluorescent signal remained unchanged

over a period of 2 weeks in all media used and show optimal emission in mouse serum. When the ABF microrobots were injected in the intra-peritoneal cavity of a 4-week-old Balb/C mouse (Figure 3Fi), a fluorescent signal from the ABF microrobots could be detected in the lower part of the abdominal cavity consistent with the location of the injected ABF microrobots (Figure 3Fii). When propelled toward the lower part of the animal body (i.e., lab mice) in a rotational magnetic field, the NIR-ABF microrobots can emit red and yellow signals with the motion, as shown in images captured every minute (Figure 3Fiii). These results suggest the excellent ability of *in vivo* targeting imaging under the guidance of external magnetic field. Remarkably, such ABF

microrobots allowed whole-body fluorescence imaging for *in vivo* tracking in the peritoneal cavity of a mouse due to the use of long-wavelength dyes, opening a venue for widespread application of the microrobot-based FI.

However, dyes-functionalized micro-/nano-robots are still hampered in use by their intrinsic properties of the incorporated dyes in the long run. Most of organic dyes are incompatible and even toxic to biosystem. So far, only two fluorophores are approved by the U.S. Food and Drug Administration for medical use, indocyanine green (ICG) and fluorescein (24,49). Despite of the fact that fluorescein has been approved for human use for over 30 years, side effects are still non-negligible, such as rapid decay and hypersensitivity reactions (50). Moreover, organic dyes, such as fluoresceins, rhodamines and most cyanins, have limited applications in long-term imaging and multi-color detection due to their insensitive Stoke shifts, low molar absorption coefficients, narrow absorption, and broad emissions with poor separation of absorption and emission bands. Their fluorescence shows poor stability in acid, saline and alkaline media, and easy to self-quenching at high concentrations and photo-bleaching under the long-time illumination. Thus, development of micro-/nano-robots functionalized with biocompatible and stable fluorescent dyes is a promising direction.

Quantum dots (QDs) are a new emerging family of nanomaterials with all three dimensions in the range of 1–10 nm (51). Due to quantum confinement effects, QDs show outstanding optical properties, such as high quantum yields, broad absorption spectra, narrow and symmetric size-tunable emission, and strong resistance to photobleaching (52–56). Thus, QDs provide a new class of biomarkers that could circumvent the limitations of organic dyes. Since the first examples from Alivisatos (57) and Nie's groups (58), the use of QDs as luminescence tags and probes has increased significantly in the past two decades for detection and imaging in several areas in the life sciences, ranging from sensing technology to fluorescence *in situ* hybridization to *in vivo* imaging. Recently, with the improvement of newly emerging functionalized QDs, QDs-based FI is even more promising in biological research. Either QDs alone or integrated with other functional micro-/nano-structures and even micro-/nano-robots are useful as contrast reagents in fluorescence imaging or in other molecular imaging.

Jurado-Sánchez *et al.* firstly demonstrated that the coupling of the optical properties of QDs and the autonomous movement of artificial nanomachines offers a novel approach to the real-time optical visualization of the analyte recognition events (*Figure 4A*) (59). Tubular

microrobots were decorated with multiple CdTe QDs by electrostatic self-assembly, leading to mobile QD-based microrobots (*Figure 4B*). As a result, the movement of such microrobots is observable by the FI (*Figure 4C*). Moreover, the fluorescent change can be monitored for evaluating the capability of the selective detection of a variety of toxic organic and inorganic threats (*Figure 4D*). The fluorescent intensity is tunable by increased CdTe QD loading for further *in vivo* application. Such mobile QD fluorescent platforms represent promising alternatives to conventional fluorescent dyes and may offer diverse possibilities for new future developments in *in vivo* FI.

Despite many superior fluorescent properties, the cytotoxicity of QDs and complex hybrid process with micro-/nano-robots usually limit the *in vivo* application of QD-based microrobots. To search the novel imaging agent becomes vital for future biomedical imaging. Emerging as a biocompatible and environmentally friendly nanomaterial, carbon quantum dot with good optical properties and biocompatibility have been studied extensively for *in vitro* and *in vivo* bioimaging (38,61,62). It is reported that such QDs can be easily integrated onto the fabrication of the micro-/nano-robots due to good water solubility. Jurado-Sánchez *et al.* adopted a bottom-up approach to introduce a huge loading of fluorescent graphene quantum dots (GQDs) into the Janus micromotor body (*Figure 4E*) (60). The resulting microrobots exhibited strong, well-distributed blue fluorescence emission, which can be used to track their movement under dark field (*Figure 4F,G*). Moreover, the fluorescent change can be employed to evaluate the detection of bacteria endotoxins (*Figure 4H*). As stated above, the functionalized micro-/nano-robots with GQDs show good fluorescent emission, but they are mainly used for targeting detection by FI (63,64). If these microrobots are planned to use for targeting imaging, they must be magnetized with magnetic nanomaterials for steering to the destined location.

Compared to established organic dyes, the QD-functionalized micro-/nano-robots show size-tunable absorption and emission, high fluorescence quantum yields even in the NIR wavelengths and large two-photon action cross-sections. Nevertheless, there are yet some limitations to be addressed. Firstly, the solutions for using QDs have so far been individual organic ones. The property of QDs is quite different compared with dye molecules, which complicates their functionalization process of micro-/nano-robots and their application in physiological environments. Secondly, the cytotoxicity of QDs is usually a significant concern before their application to cellular or *in vivo* study,

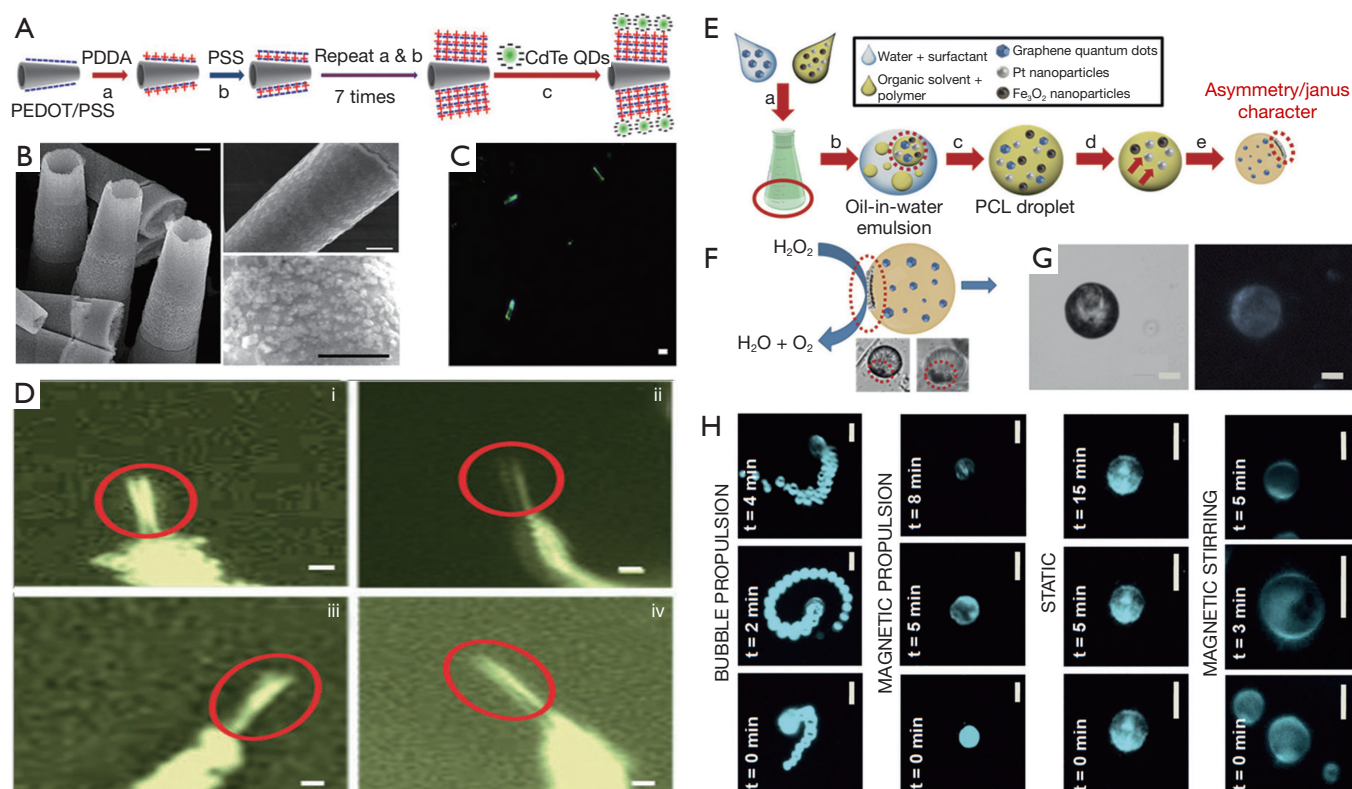


Figure 4 Quantum dot (QD)-based microrobots. (A) Preparation process of QD-based microrobots from layer-by-layer self-assembly of COOH-CdTe QDs on PEDOT microrobots. (B) SEM images of QD-based microrobots. (C) Fluorescence microscopy images of the microrobots. (D) Fluorescent images of a QD-based microrobot before (i) and after 30 s locomotion in solutions containing Hg^{2+} (3 mg/L) (ii), Pb^{2+} and Cu^{2+} (5 mg/L) (iii) or methylmercury (5 mg/L) (iv). Scale bar is 2 mm (59). (E) Preparation procedure of the graphene quantum dot (GQD) Janus microrobots (60). (F) Asymmetry and Janus character of the microrobots (60). (G) Optical and fluorescence image ($\lambda_{\text{ex}}=360$ nm, $\lambda_{\text{em}}=470$ nm) of the microrobots. (H) Successive images show the fluorescence of moving and static microrobots (60). Reprinted with permission from Copyright 2015 RSC (59), Copyright 2017 Wiley (60). PDDA, poly dimethyl diallyl ammonium chloride; PEDOT, poly (3,4-ethylenedioxythiophene); PSS, poly (sodium-p-styrenesulfonate); PCL, polycaprolactone.

especially cadmium-containing semiconductor quantum dots (65). Their toxicity hampers their further practical applications to great extent. Although more biocompatible QDs with multi-color luminescence emissions, such as cadmium-free quantum dots and carbon quantum dots, have been successfully synthesized, their integration with micro-/nano-robots for clinic applications still keep challenging.

Based on the long history of fluorescence imaging in medicine and the emerging imaging using robots, the fluorescence-based micro-/nano-robots has found tremendous interest in bioimaging because the FI is high sensitivity, high selectivity, convenience, diversity and non-destructive character (66). More important, such an imaging ability depends on the modified fluorescent agents (67-70). Consequently, the development of the

fluorescence-based micro-/nano-robots is also limited by fluorescent agents including organic dyes, autofluorescence materials and quantum dots. Moreover, FI, as a kind of optical imaging, generally use the visible light for imaging, which is more or less constrained by the parameters of lights. As it is known, visible light has an inherently low capacity for penetrating biological tissue and experiences significant scattering in biological media (52). The use of current fluorescence-based 2D and 3D techniques for whole-body *in vivo* imaging is limited to superficial areas, just below the skin or the surface of internal organs and cavities. Visualization through the skin is restricted to superficial tissues such as the breast or lymph nodes (71-73). Thus, further visualization of deep tissues may need the combination with endoscopy or surgery. It is also necessary

to search the long-wavelength, even near infrared region, fluorescent agents for deep-tissue imaging. In addition, the integration of fluorescent agents with micro-/nano-robots is still challenging, whatever surface modification or internal encapsulation. Such integration obtain the fluorescent micro-/nano-robots inherited the merits from two components, but make some individual features lost and increase the complexity of targeting imaging. How to balance them is critical for high-performance targeting *in vivo* imaging. Overall, based on the high sensitivity, high selectivity, diversity and non-destructive features of the , it is a good choice and strategy for the localization of the micro-/nano-robots at the tissues near the skin to avoid both the limited penetration of the fluorescence and the interference from autofluorescence of tissue.

RI

As another kind of important imaging technique, RI offers the potential for whole body scanning due to highly sensitivity and quantitative feature (74,75). It generally includes γ scintigraphy, PET and SPECT (76,77). These tomography imaging techniques have been extensively utilized in clinical settings, where they serve for the early diagnosis and the evaluation of patient responses to therapy for a variety of diseases. The imaging abilities mainly rely on the introduction of exogenous agents-radionuclides, which directly emit (in SPECT) or indirectly generate gamma (γ) rays in the positron-electron annihilation process (in PET). Due to a high penetration capacity of γ rays for biological tissue possess, PET and SPECT methods can upscale easily from small experimental animals to humans, without encountering any significant issues related to tissue-attenuation. Moreover, γ rays can be traced in real time once being administered into the body for minutes or hours, which provides information about the activity of biological processes. Like fluorescent micro-/nano-robots, novel micro/nano-robots based on RI can be obtained by the easy encapsulation of positron or gamma emitters, which is also suitable for real-time tracking and targeting medical imaging.

Very recently, Vilela *et al.* demonstrated the PET-CT imaging ability of the ^{124}I -functionalized bubble-propelled tubular micromotors for their tracking (Figure 5A,B) (19). A large population of catalytic self-propelled microrobots was firstly synthesized by template-directed electrodeposition protocol and following metal evaporation (Figure 5C). The synthesized microrobots were radiolabeled on their gold surface via chemisorption of iodine-124 (Figure 5C). This

labeling strategy renders the microrobots detectable by PET, which is applicable to future *in vivo* studies. The related imaging studies were demonstrated in linear phantoms, as shown in Figure 5D. It is observed that the movement of the catalytic microrobots becomes visible in SDS/H₂O₂ when tracking their location using positron-emission tomography in combination with X-ray CT (Figure 5E). The PET-CT images using the functionalized microrobots offer dynamic quantitative information on the temporal evolution of their spatial distribution within the phantoms, in good agreement with the observations obtained using optical microscopy (Figure 5F). In conclusion, imaging large amounts of functionalized catalytic microrobots moving in confined channels could show a great promising in PET-CT imaging. This study represents a great step toward the tracking of microrobots using current medical imaging technology for *in vivo* applications, making the functionalized microrobots for medical imaging in the foreseeable future.

The studies of the microrobots related to RI application are just emerging, which has a long way to go. On the one hand, radionuclides (radioactive compounds) have an intrinsically limited half-life and expose the patient and practitioner to ionizing radiation (78), therefor are subject to a variety of stringent safety regulations which limit their repeated and extensive use. Moreover, the amount of emitted radioactivity is directly proportional to the labeled species concentration. The modification of the microrobots with these high-loading radionuclides is still challenging for *in vivo* application when balancing safety and performance. On the other hand, although RI techniques are considered minimally invasive, ultrasensitive, and allow for a time-resolved and quantitative determination of the amount of labeled species at the whole-body level, they have poor spatial and temporal resolution and offer poor morphological information (79), thus are frequently used in combination with anatomical techniques (i.e., CT). It is indispensable to develop the microrobots with multimodal imaging.

MRI

For the magnetic field actuated micro- and nanorobots, the visualization of the micro- and nanorobots is a very important issue, especially for their locomotion inside the blood vessels. Some people may suggest that the micro- and nanorobots with magnetic property *in vivo* can be controlled and guided with a permanent magnet placed outside the body. However, the magnet shows a lot of difficulties for the controlling of the tiny robots because the magnet

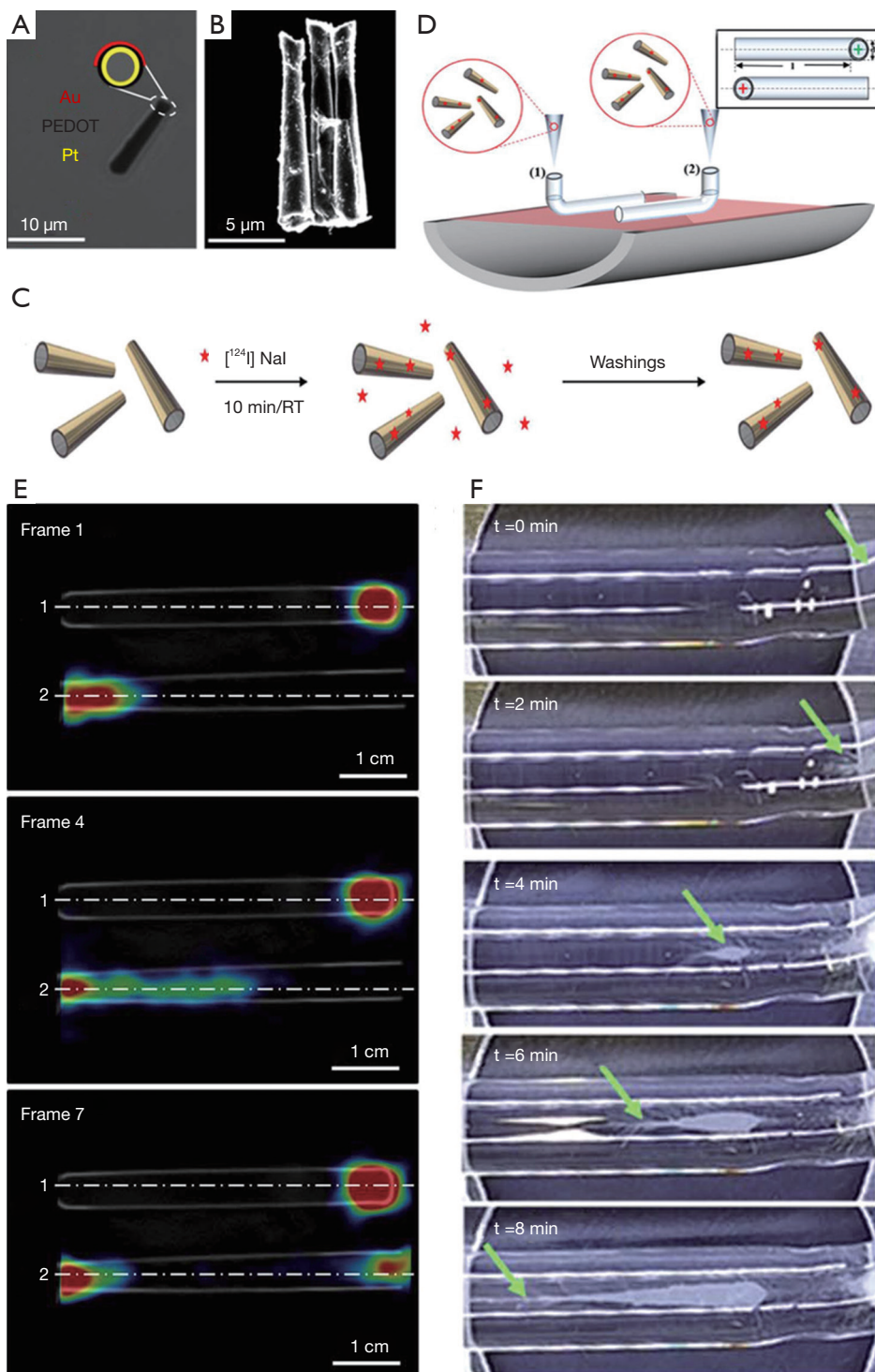


Figure 5 Radionuclide-labeling microrobots. (A) Optical image of Au-microrobots. (B) SEM image of Au-microrobots. (C) Schematic illustration of the preparation process of Au-microrobots. (D) Phantoms for positron emission tomography in combination with computed tomography (PET-CT) imaging of Au-microrobots. (E) PET-CT images corresponding to frames 1, 4, and 7. (F) Optical images show the self-propelled Au-microrobots navigating over time inside the phantom tubes (19). Reprinted with permission from Copyright 2018 ACS (19).

must be placed quite close to the micro- and nanorobots to generate sufficient attraction to them and the attraction force may only possess one direction. Moreover, the uneven magnetic field generated by a magnet makes the micro- and nano-robots easily be accelerated to unmanageable speed and make them untraceable. Therefore, researchers have developed several types of electromagnetic coils systems to generate on-demand magnetic fields to control the micro- and nano-robots in 1D, 2D and 3D motions, so that the magnetic micro- and nano-robots can adapt the complex fluid environment *in vivo*, especially for the complex maze of vessels. As a kind of external field propelled micro- and nano-robots, the magnetic micro- and nano-robots can be either powered by the magnetic field itself or powered by the other ways but steered by the magnetic field (80-82). The geometry structure of the micro- and nano-robots contains helical structures, rigid head with flexible tails, rigid wires, U-shape bricks and others (47,83-98). To precisely control the micro- and nanorobots to a targeted region, we must know the precise position of the micro- and nano-robots. MRI is a very efficient tool to visualize the magnetic micro- and nanorobots both *in vitro* and *in vivo* with high contrast, which has several advantages than the other kinds of imaging methods especially for CT. First, MRI does not generate ionizing radiation to human body. Second, MRI can obtain the 3D section imaging without reconstruction process. Third, it shows a better imaging contrast of soft tissue, such as bladder and bowel, and higher resolution of imaging than CT.

The MRI machine is mainly composed with a doughnut-shaped superconducting magnet with a radio-frequency coil located inside, transmits radio-frequency waves and collects the radio-frequency signals. Mostly, hydrogen atoms are selected to generate radio-frequency signals that are collected by the antennas of the MRI. While the transmitted wave frequency of the MRI matches the spin rate of the protons, the spin direction converted. And while the transmitted wave stopped, the protons relaxed back to the original low energy states and emitted radio signals, which is called relaxation. The emitted radio signals would be collected and recorded by the MRI system. With the changing of the pulse sequence, differentiable imaging contrast can be obtained between different tissues due to the relaxation properties of the hydrogen atoms inside. Basically, two kind of relaxation processes are utilized to generate the MRI, i.e., longitudinal relaxation (T1-recovery) and transverse relaxation (T2-recovery). The former one generates bright contrast and the later one

generates dark contrast in MRI, respectively. The magnetic micro- and nano-robots assembling with superparamagnetic nanoparticles generally serve as T2 contrast agents to offer a dark MRI. The contrast enhancement is positively related to the magnitude of the magnetization. It is reported that the resolution of the MRI can reach up to about 100 μm depended on the strength of the magnetic field (99).

Both the natural and artificial magnetic micro- and nano-robots have been reported. Magnetotactic bacteria are a group of bacteria that can align themselves with the Earth's magnetic field. Under a magnetic field, the bacteria can adapt their moving orientation via a chain of iron oxide nanoparticles wrapped with lipid membrane called magnetosomes that served as a compass needle (100). Benoit *et al.* (101) found that the magnetotactic bacteria show the instinctive tendency to the tumors in mice inspected by the MRI. Martel *et al.* (102-109) investigated the motion of the magnetotactic bacteria which contains two flagellar bundles with tagged magnetic microscale particles. Under the magnetic steering, the magnetotactic bacteria transport through the microvasculature for directed chemotherapy under MRI. They developed a medical interventional platform that apply MRI as the imaging modality for feeding back information to controller which is responsible for the real-time locomotion of the magnetotactic bacteria and the artificial micro- and nano-robots along pre-planned paths in the blood vessels to perform targeted delivery tasks, as illustrated in *Figure 6* (104). They also (110) harnessed the magnetococcus marinus as the drug carrier to adhere and deliver cancer drug SN-38 loaded liposomes. Under the magnetic field the injected bacteria are successfully guided to the tumor with high proportion and they release their drugs to the tumor hypoxic regions after the bacteria dead. Martel *et al.* (103,111) demonstrated that the polar magnetotactic bacterial nanorobots show the capability to load cargos under the MRI system for tracking purpose which is hardly detectable with other kinds of imaging methods. They suggested that their steerable magnetotactic bacteria are applicable for the treatment of cancer and thrombus with MRI for medical imaging.

To mimic the magnetotactic bacteria, researchers also developed artificial magnetic micro-/nano-robots that are actuated with magnetic field and visualized under MRI. Behkam *et al.* (112) developed a kind of swimming microrobot which contains two-phase stepper motor, Styrofoam jacket, and steel wire. The design is inspired from the peritrichous flagellation propulsion of bacteria and the microrobot can be actuated in low speed biofluids under

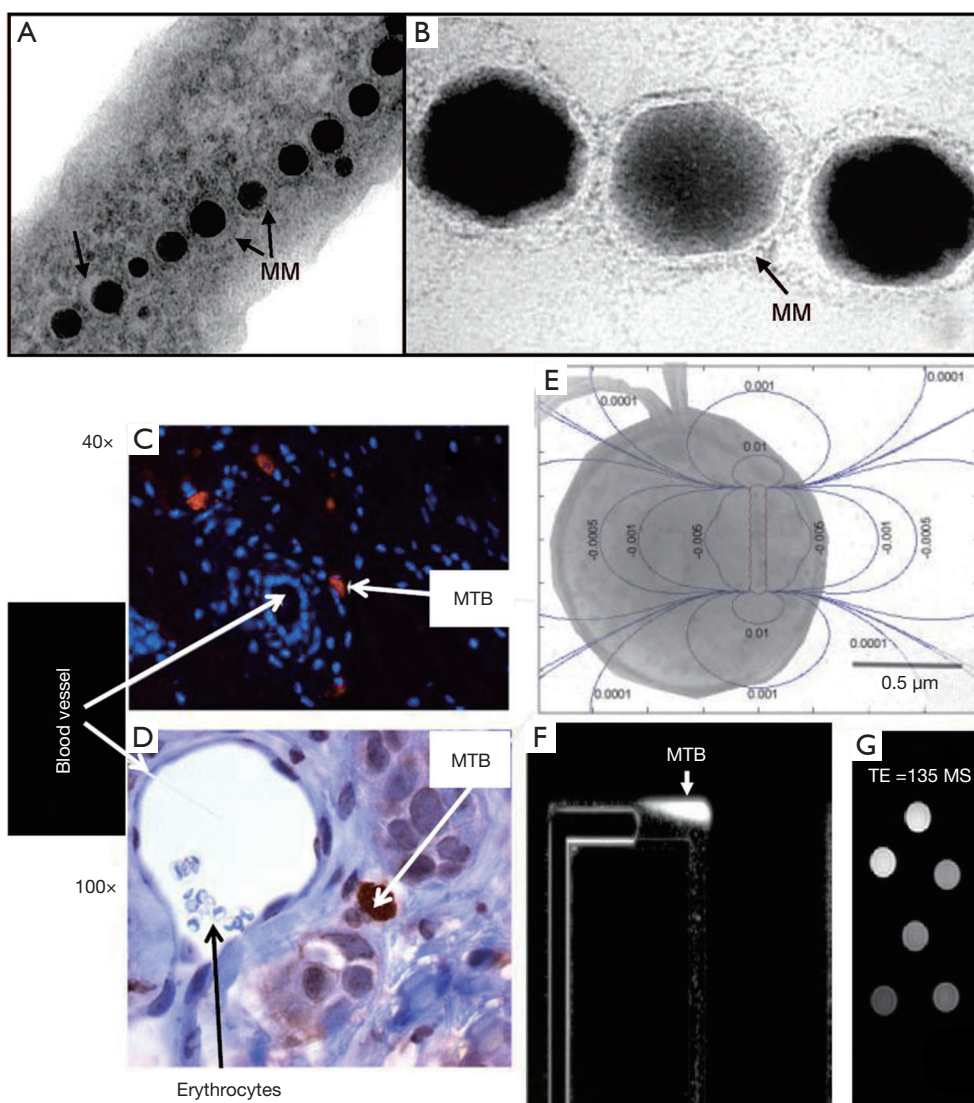


Figure 6 Localization of magnetotactic bacteria with MRI. (A) and (B) TEM image show the magnetotactic bacteria (*M. gryphiswaldense*) and the magnetosomes inside the bacteria (100). (C) and (D) shows the microscopy images of the bacteria after a targeting process to the interstitial region of a tumor with magnifications of 40 \times and 100 \times respectively. (E) Electron microscope image of one magnetotactic bacteria that contains a chain of magnetosomes two flagella with the superposed distortion of the spatial magnetic field expressed in ppm. (F) Magnetotactic bacteria swarm which is actuated along pre-determined paths in microchannels. (G) Various concentrations of magnetotactic bacteria imaged with a clinical magnetic resonance imaging (MRI) system (104). Reprinted with permission from Copyright 2008 ACS (100), Copyright 2009 SAGE (104). MM, magnetosome membrane; MTB, magnetotactic bacteria.

MRI. Yan *et al.* (16) fabricated a kind of biohybrid magnetite helical microrobots by applying the *Spirulina* microalgae as the template. The kind of microrobots can be tracked using not only the fluorescence imaging, but also the MRI *in vivo* as shown in Figure 7. The dual mode imaging of the biohybrid microrobots may facilitate the *in vivo* imaging-guided therapy.

Because the enhancement of the MRI contrast of *in vivo* tissues by ferromagnetic micro- and nano-robots MRI have been proved, the micro- and nano-robots robots with magnetism show their potential for the *in vivo* localization with MRI by repeated navigation under magnetic actuation system and inspection with MRI as feedback for the next step navigation.

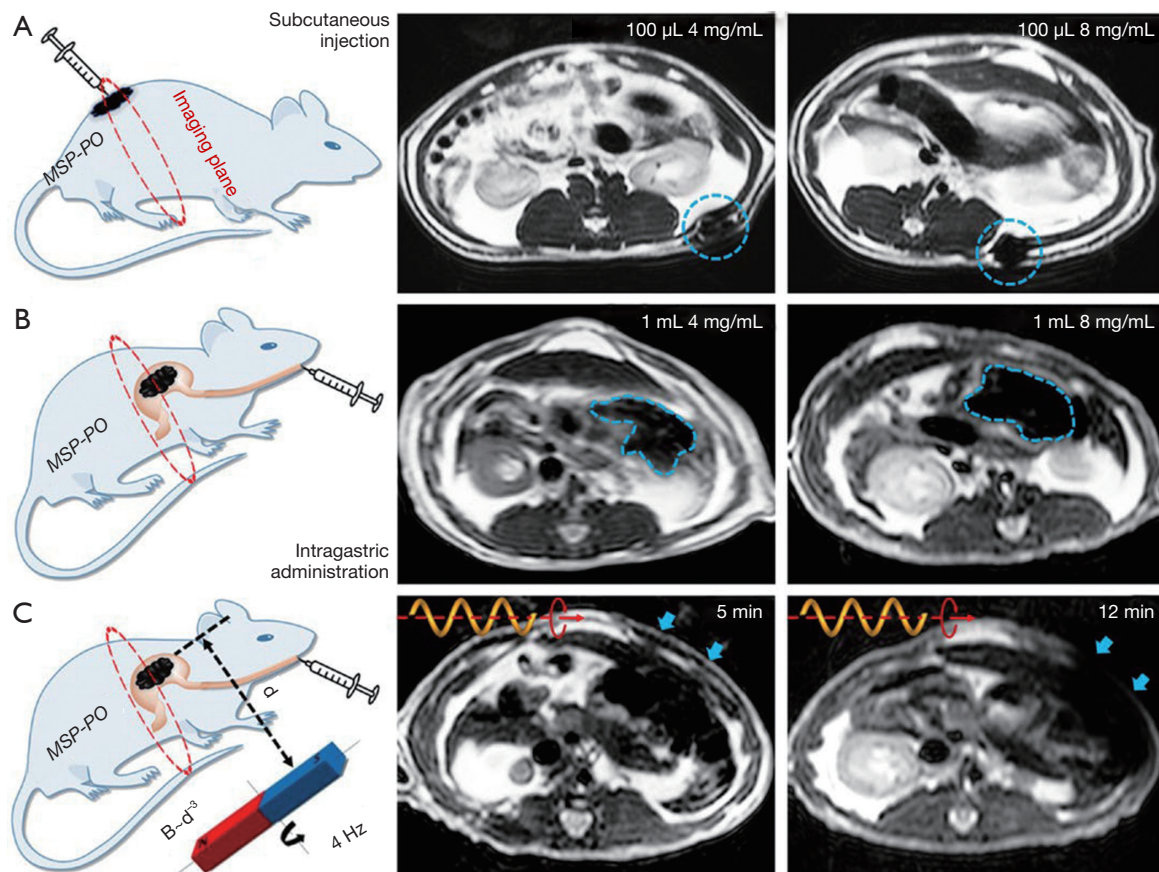


Figure 7 Cross-sectional magnetic resonance imaging (MRI) of swarm of magnetized *S. platensis* in Sprague-Dawley rats. (A) T2-weighted MRI of warm of magnetized *S. platensis* inside the subcutaneous tissues with concentrations of 4 and 8 mg/mL. (B) T2-weighted MRI of swarm of magnetized *S. platensis* inside the stomach with concentrations of 4 and 8 mg/mL. (C) MRI of magnetized *S. platensis* swarm with different time periods of the stomach of rat. The magnetic actuation and MRI are applied with a sequence (16). Reprinted with permission from Copyright 2017 AAAS (16).

US imaging

Except for tracking and location of microrobot using magnetic resonance (MR), CT, etc., because of real-time control of image feedback, no unfavorable effects on health, low cost for mature commercial diagnosis, US imaging stands out as a promising alternative among above medical imaging techniques for medical robotics. US has relatively deeper imaging depths of about 10 cm with human tissue and possible resolution of submillimetric accuracy, which enable it to detect and localize a single microbubble to trace the microrobots; while other clinical modalities like MRI and CT, they need micromolar to millimolar levels of contrast agent to detect the targets. Such great benefits of US make it a high-efficiency method in control of microrobots *in vivo* potentially.

Sanchez *et al.* (113) reported the control of self-propelled microjets using ultrasound equipment, in which the propulsion of microjets is due to continuous ejection of oxygen (O_2) bubbles originated from a catalytic reaction on their inner platinum surface in present of hydrogen peroxide (H_2O_2). The microjet has fastest speeds up to 200 body lengths per second. This kind of microrobot can be controlled not only by their self-propulsion, but also by the external magnetic field (especially under a weak magnetic gradient). As a result, by tracing the position of microbubble through the magnetic torques, the microjets can be steered to motion from one point to another defined point. Ultrasound B-model image feedback experiments showed that the microjets can motion relatively precisely following two different closed-loop trajectories (diamond shape and figure-eight shape) with an average velocity of $156 \pm 35.1 \mu\text{m/s}$

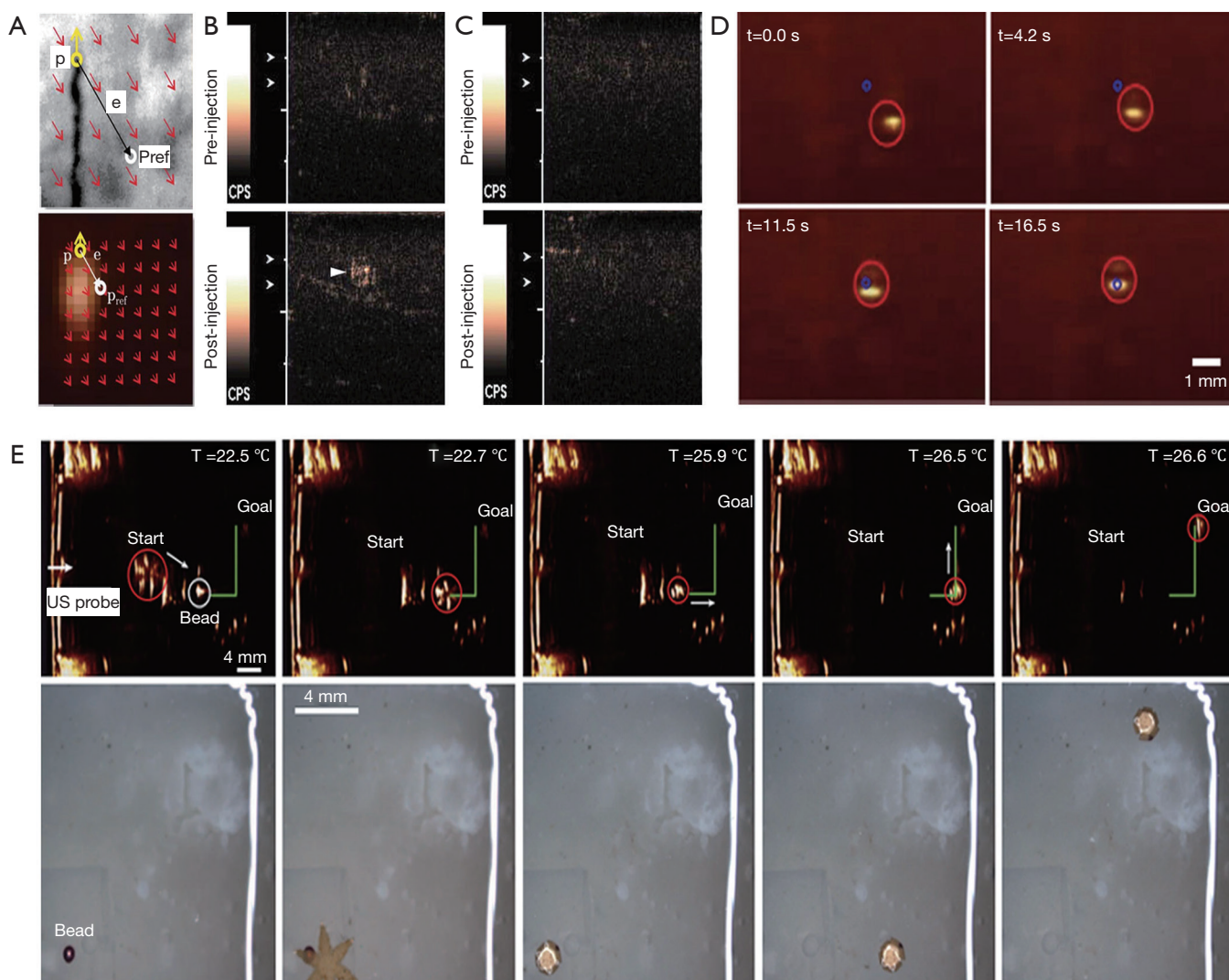


Figure 8 Localization of microrobots with US imaging. (A) Magnetic actuation and control of self-propelled microjets under ultrasound image guidance. Magnetic field line is presented with red line; yellow circles with arrow show the instantaneous position and velocity (113). (B,C) The contrast mode ultrasound about *in vivo* experiment of nanosphere converters (NSCs) and control nanospheres injected at the site of an abscess, respectively. (B) NSCs injected at abscess margin (top) results in a discernable increase in signal on contrast mode ultrasound (bottom, yellow arrowhead); (C) control nanospheres lacking catalase injected in similar location (top) resulted in no appreciated signal (bottom) (114). (D) Controlled movement of a microparticle by applying ultrasound feedback (115). (E) Successive ultrasonic (US) images (top) and successive microscopic images (bottom) of the soft miniaturized gripper during manipulation and transportation of a bead. Once the gripper reaches the target, the temperature is increased to make the gripper closed. After that, a pre-defined trajectory guides the gripper to the target region (116). Reprinted with permission from Copyright 2014 IEEE (113,115), Copyright 2017 IEEE (117), Copyright 2013 Elsevier (114).

and with an average tracking error of $250.7 \pm 164.7 \mu\text{m}$. However, this location accuracy is somewhat lower than that of microscopic image feedback, which is $207 \pm 25.9 \mu\text{m/s}$ and $183.2 \pm 84.31 \mu\text{m}$, respectively (Figure 8A).

Much deeper and more meticulous work about detection of microbubble produced by micromotors with ultrasound

molecular imaging is done by Olson and co-workers (114). They prepared efficient micromotors converters (MMCs) and nanosphere converters (NSCs) that both can produce O_2 microbubbles by catalyzing H_2O_2 . *In vitro* experiments showed that for MMCs, microbubbles can be detected using ultrasound feedback at a much lower H_2O_2 levels of

0.8 mM, while with the microscopy system, it needs the lowest H_2O_2 levels of 65.3 mM. Furthermore, by adding activated neutrophils to catalase-layered NSCs, the team successfully detected the microbubbles and found 8–60 μM H_2O_2 produced in neutrophils. For contrast, the NSCs without catalase layer are not able to interact with activated neutrophils to detect the microbubbles. Based on above work, finally, NSCs were tested in an *in vivo* model of abscess in rats finally. Abscesses were characterized by the presence of a large number of activated neutrophils that release H_2O_2 . For contrast, both control nanospheres and NSCs were injected under ultrasound guidance at the abscess margin sequentially. Also, the same procedure was done on normal rat thigh muscle. The results suggested that only when the NSCs were injected in abscesses, the microbubble production signal can be detected, which suggested that the elevated levels of H_2O_2 are required. This *in vivo* experiment showed great application of ultrasound imaging-based control of micromotors in medicine (Figure 8B,C).

Referring to non-self-propelled microrobot, Khalil *et al.* (115) did the study based on paramagnetic microparticles and ultrasound feedback (Figure 8D). By investigating the relation between the magnetic field, field gradient and the applied current at electromagnets, it is provided that the magnetic field gradient is almost uniform in the workspace during the implementation of the ultrasound-based closed-loop control of the microparticles. The results indicated that the microparticles can be pulled in all directions within the workspace and the motion can be point-to-point control. Via this control system, the paramagnetic microparticles achieve the three motion trajectories, that is, sinusoidal trajectory, S-trajectory and zig-zag trajectory. The positioning accuracy-based ultrasound feedback has an average tracking error of $48 \pm 59 \mu\text{m}$, whereas, the control system based on microscopic system has an average tracking error of $21 \pm 26 \mu\text{m}$.

To manipulate and transport biological materials in tortuous environments, Scheggi *et al.* prepared a kind of soft miniaturized untethered grippers which was thermally responsive (116). By regulating the temperature of environment wherein the grippers exited, the miniaturized grippers can achieve from unfolded 2D flat shape to 3D folded shape to realize the grasp and put-down ability. Moreover, the grippers' material contained 3% (w/w) Fe_2O_3 , so that they could be responsive to magnetic fields. In the study, the gripper can be controlled to motion using ultrasound feedback along both step path and sinusoidal path (Figure 8E). Much nimbly, the gripper could move

from the initial position toward a target area in a cluttered environment, which indicated that the gripper has great potential to work in a much complex real case. Exhilaratingly, this soft miniaturized untethered gripper showed ability to grasp a 0.5 mm bead and transport it along a path until a target area is reached. Results indicates that the control system employing ultrasound images has an average tracking error of $0.4 \pm 0.13 \text{ mm}$ without payload and $0.36 \pm 0.05 \text{ mm}$ when the agent performs a transportation task with a payload.

From these studies, it is known that using ultrasound feedback to monitor the motion of microrobots has great applications in medical diagnosis and it can provide possible accuracy and real-time control without harm in situations that some other visual feedback cannot be provided or unsuitable.

Conclusions and outlook

To realize the clinical applications of micro-/nano-robots, the integration of the navigation and localization techniques of the micro-/nano-robots is indispensable. The advantages and disadvantages of various kinds of imaging modes are summarized in Table 1. Different imaging techniques have their specific merits on imaging. FI and RI show its advantage in the high sensitivity. MRI shows its advantage in nonionizing radiation. US imaging shows its advantage in noninvasive feature. The current imaging modes generally possess insufficient resolution to visualize the micro- and nano-robots, especially for the nano-scale robots. Some of the imaging techniques require to apply contrast agents to generate sufficient contrast between disease site, different tissues and the micro- and nanorobots. The retention of the contrast agent may show long-term cytotoxicity to the tissues and organs. For the RI, the radioactive isotopes used in radiology and ionizing radiation may injure the surrounding tissues at high concentrations and prolonged using time. For micro- and nanorobots under MRI, the treated patients should be excluded from those who have cardiac pacemakers and metallic foreign bodies. To address the above imperfection, different imaging techniques should be applied in different cases, according to the specific site for imaging and the personal details of the patient.

The future focus on the development of integrating imaging modality with robotics for clinic applications may divide into the following three aspects. The first aspect is to improve the resolution of the imaging techniques from micro-scale to submicro- and nano-scale. The second aspect may focus on the enhancement of the contrast of the micro-

Table 1 Summary of common bioimaging modalities for tracking the functionalized microrobots *in vivo*

Mode	Imaging probe	Pros	Cons
FI	Micro-/nanorobots decorated with fluorescent dyes and nanoparticles	Good planar resolution (≈ 100 nm); high sensitivity	Shallow imaging depth (≈ 2 mm); poor biocompatibility and biodegradability
RI	Radioactive tracer functionalized micro-/nanorobots	High sensitivity; fast imaging time	Low spatial resolution ($\approx 1-2$ mm); ionizing radiation
MRI	Magnetic micro-/nanorobots	Nonionizing radiation; high soft tissue contrast	High cost; long imaging time
US imaging	Micro/nanorobots generating microbubbles	Noninvasive, portable, low-cost, safe, fast	Limited penetration/sensitivity, low signal noise ratio, low resolution; interfered by bone

and nano-robots compared with the surrounding tissues, from both the design of the micro- and nano-robots, and the collective behavior of the robots through reconfigurable swarming process (117,118). The third aspect is to develop the micro- and nano-robots that can be imaged with multi-modalities. Therefore, the imaging strategies of the micro- and nano-robots for their *in vivo* application can be collaborated and switched according to the real case.

Acknowledgements

Funding: This work was partially supported by the early career scheme (ECS) grant and General Research Fund (GRF) from the Research Grants Council (RGC) of Hong Kong with Project nos. 439113, 14209514, 14203715 and 14218516, and the funding from CUHK T Stone Robotics Institute.

Footnote

Conflicts of Interest: The authors have no conflicts of interest to declare.

References

- Nelson BJ, Kallakatsos IK, Abbott JJ. Microbots for minimally invasive medicine. *Annu Rev Biomed Eng* 2010;12:55-85.
- Wang J, Gao W. Nano/microscale motors: Biomedical opportunities and challenges. *ACS Nano* 2012;6:5745-51.
- Gao W, Wang J. The environmental impact of micro/nanomachines: A review. *ACS Nano* 2014;8:3170-80.
- Palagi S, Fischer P. Bioinspired microrobots. *Nat Rev Mater* 2018;3:113-24.
- Sitti M. Miniature soft robots — road to the clinic. *Nat Rev Mater* 2018;3:74-75.
- Yang G, Bellingham J, Dupont P, Fischer P, Floridi L, Full R, Jacobstein N, Kumar V, McNutt M, Merrifield R, Nelson B, Scassellati B, Taddeo M, Taylor R, Veloso M, Wang Z, Wood R. The grand challenges of Science Robotics. *Sci Robot* 2018;3:ear7650.
- Sitti M, Ceylan H, Hu W, Giltinan J, Turan M, Yim S, Diller E. Biomedical applications of untethered mobile milli/microrobots. *Proc IEEE Inst Electr Electron Eng* 2015;103:205-24.
- Xu L, Mou FZ, Gong HT, Luo M, Guan JG. Light-driven micro/nanomotors: from fundamentals to applications. *Chem Soc Rev* 2017;46:6905-26.
- Peng F, Tu YF, Wilson DA. Micro/nanomotors towards *in vivo* application: cell, tissue and biofluid. *Chem Soc Rev* 2017;46:5289-310.
- Peyer KE, Zhang L, Nelson BJ. Bio-inspired magnetic swimming microrobots for biomedical applications. *Nanoscale* 2013;5:1259-72.
- Xu B, Zhang B, Wang L, Huang G, Mei Y. Tubular Micro/Nanomachines: From the Basics to Recent Advances. *Adv Funct Mater* 2018;28:1705872.
- Wang H, Pumera M. Micro/Nanomachines and Living Biosystems: From Simple Interactions to Microcyborgs. *Adv Funct Mater* 2018;28:1705421.
- Shao L, Kall M. Light-Driven Rotation of Plasmonic Nanomotors. *Adv Funct Mater* 2018;28:1706272.
- Safdar M, Khan SU, Janis J. Progress toward Catalytic Micro- and Nanomotors for Biomedical and Environmental Applications. *Adv Mater* 2018;30:e1703660.
- Guix M, Mayorga-Martinez CC, Merkoci A. Nano/Micromotors in (Bio) chemical Science Applications. *Chem Rev* 2014;114:6285-322.
- Yan X, Zhou Q, Vincent M, Deng Y, Yu J, Xu J, Xu T, Tang T, Bian L, Wang YX, Kostarelos K, Zhang L.

- Multifunctional biohybrid magnetite microrobots for imaging-guided therapy. *Sci Robot* 2017;2:eaq1155.
17. Wen S, Zhao L, Zhao Q, Liu C, Yu Z, Shen M, Majoral J, Mignani S, Zhao J, Shi X. A promising dual mode SPECT/CT imaging platform based on ^{99m}Tc-labeled multifunctional dendrimer-entrapped gold nanoparticles. *J Mater Chem B* 2017;5:3810-5.
 18. Kesner S, Howe RD. Robotic catheter cardiac ablation combining ultrasound guidance and force control. *Int J Rob Res* 2014;33:631-44.
 19. Vilela D, Cossío U, Parmar J, Martínez-Villacorta AM, Gómez-Vallejo V, Llop J, Sánchez S. Medical Imaging for the Tracking of Micromotors. *ACS Nano* 2018;12:1220-7.
 20. Wolfbeis OS. An overview of nanoparticles commonly used in fluorescent bioimaging. *Chem Soc Rev* 2015;44:4743-68.
 21. Wen CY, Xie H, Zhang Z, Wu L, Hu J, Tang M, Wu M, Pang D. Fluorescent/magnetic micro/nano-spheres based on quantum dots and/or magnetic nanoparticles: preparation, properties, and their applications in cancer studies. *Nanoscale* 2016;8:12406-29.
 22. Bu L, Shen B, Cheng Z. Fluorescent imaging of cancerous tissues for targeted surgery. *Adv Drug Deliv Rev* 2014;76:21-38.
 23. Hsiang JC, Jablonski AE, Dickson, RM. Optically Modulated Fluorescence Bioimaging: Visualizing Obscured Fluorophores in High Background. *Acc Chem Res* 2014;47:1545-54.
 24. Kobayashi H, Ogawa M, Alford R, Choyke PL, Urano Y. New Strategies for Fluorescent Probe Design in Medical Diagnostic Imaging. *Chem Rev* 2010;110:2620-40.
 25. Kim D, Kim J, Park YI, Lee N, Hyeon T. Recent Development of Inorganic Nanoparticles for Biomedical Imaging. *ACS Cent Sci* 2018;4:324-36.
 26. Shang L, Dong S, Nienhaus GU. Ultra-small fluorescent metal nanoclusters: synthesis and biological applications. *Nano Today* 2011;6:401-18.
 27. Han DW, Matsumura K, Kim B, Hyon SH. Time-dependent intracellular trafficking of FITC-conjugated epigallocatechin-3-O-gallate in L-929 cells. *Bioorg Med Chem* 2008;16:9652-9.
 28. Wu X, Liu H, Liu J, Haley KN, Treadway JA, Larson JP, Ge N, Peale F, Bruchez MP. Immunofluorescent labeling of cancer marker Her2 and other cellular targets with semiconductor quantum dots. *Nat Biotechnol* 2003;21:41-6.
 29. Ma Y, Su H, Kuang X, Li X, Zhang T, Tang B. Heterogeneous nanometal-organic framework fluorescence probe for highly selective and sensitive detection of hydrogen sulfide in living cells. *Anal Chem* 2014;86:11459-63.
 30. Christensen J, Norgaard L, Bro R, Engelsen SB. Multivariate autofluorescence of intact food systems. *Chem Rev* 2006;106:1979-94.
 31. Billinton N, Knight AW. Seeing the wood through the trees: A review of techniques for distinguishing green fluorescent protein from endogenous autofluorescence. *Anal Biochem* 2001;291:175-97.
 32. Hall MD, Simeonov A, Davis MI. Avoiding Fluorescence Assay Interference-The Case for Diaphorase. *Assay Drug Dev Technol* 2016;14:175-9.
 33. Croce AC, Bottiroli G. Autofluorescence spectroscopy and imaging: a tool for biomedical research and diagnosis. *Eur J Histochem* 2014;58:2461.
 34. Pai JH, Wang Y, Salazar GT, Sims CE, Bachman M, Li GP, Allbritton NL. Photoresist with Low Fluorescence for Bioanalytical Applications. *Anal Chem* 2007;79:8774-80.
 35. Cao C, Birtwell SW, Høgberg J, Morgan H, Wolff A, Bang DD. Gold Nanoparticles-Coated SU-8 for Sensitive Fluorescence-Based Detections of DNA. *Diagnostics* 2012;2:72-82.
 36. Steager EB, Sakar MS, Magee C, Kennedy M, Cowley A, Kumar V. Automated biomanipulation of single cells using magnetic microrobots. *Int J Robot Res* 2013;32:346-59.
 37. Inoue Y, Izawa K, Kiryu S, Tojo A, Ohtomo K. Diet and abdominal autofluorescence detected by in vivo fluorescence imaging of living mice. *Mol Imaging* 2008;7:21-7.
 38. Hong G, Diao S, Antaris AL, Dai H. Carbon nanomaterials for biological imaging and nanomedical therapy. *Chem Rev* 2015;115:10816-906.
 39. Kozák O, Sudolská M, Pramanik G, Cígler P, Otyepka M, Zbořil R. Photoluminescent Carbon Nanostructures. *Chem Mater* 2016;28:4085-128.
 40. Aubin JE. Autofluorescence of Viable Cultured Mammalian Cells. *J Histochem Cytochem* 1979;27:36-43.
 41. Koenig K, Schneckeburger H. Laser-induced autofluorescence for medical diagnosis. *J Fluoresc* 1994;4:17-40.
 42. Terai T, Nagano T. Small-molecule fluorophores and fluorescent probes for bioimaging. *Pflugers Arch* 2013;465:347-59.
 43. Waggoner A. Fluorescent labels for proteomics and genomics. *Curr Opin Chem Biol* 2006;10:62-6.
 44. Resch-Genger U, Grabolle M, Cavaliere-Jaricot S, Nitschke R, Nann T. Quantum Dots Versus Organic Dyes as Fluorescent Labels. *Nat Methods* 2008;5:763-75.
 45. Chen M, Yin M. Design and Development of Fluorescent

- Nanostructures for Bioimaging. *Prog Polym Sci* 2014;39:365-95.
46. Yang Y, Zhao Q, Feng W, Li F. Luminescent Chemodosimeters for Bioimaging. *Chem Rev* 2013;113:192-270.
 47. Mhanna R, Qiu FM, Zhang L, Ding Y, Sugihara K, Zenobi-Wong M, Nelson BJ. Artificial Bacterial Flagella for Remote-Controlled Targeted Single-Cell Drug Delivery. *Small* 2014;10:1953-1957.
 48. Servant A, Qiu F, Mazza M, Kostarelos K, Nelson BJ. Controlled In Vivo Swimming of a Swarm of Bacteria-Like Microrobotic Flagella. *Adv Mater* 2015;27:2981-8.
 49. Carr JA, Franke D, Caram JR, Perkinson CF, Askoxyllakis V, Datta M, Fukumura D, Jain RK, Bawendi MG, Bruns OT. Shortwave Infrared Fluorescence Imaging with the Clinically Approved Near-Infrared Dye Indocyanine Green. *Proc Natl Acad Sci U S A* 2018;115:4465-70.
 50. Zheng Q, Lavis DL. Development of photostable fluorophores for molecular imaging. *Curr Opin Chem Biol* 2017;39:32-38.
 51. Selvan ST, Tan TT, Yi DK, Jana NR. Functional and Multifunctional Nanoparticles for Bioimaging and Biosensing. *Langmuir* 2010;26:11631-41.
 52. Li J, Zhu JJ. Quantum dots for fluorescent biosensing and bio-imaging applications. *Analyst* 2013;138:2506-15.
 53. Michalet X, Pinaud FF, Bentolila LA, Tsay JM, Doose S, Li JJ, Sundaresan G, Wu AM, Gambhir SS, Weiss S. Quantum dots for live cells, in vivo imaging, and diagnostics. *Science* 2005;307:538-44.
 54. Wegner KD, Hildebrandt N. Quantum dots: bright and versatile in vitro and in vivo fluorescence imaging biosensors. *Chem Soc Rev* 2015;44:4792-834.
 55. Medintz IL, Uyeda HT, Goldman ER, Mattoussi H. Quantum dot bioconjugates for imaging, labelling and sensing. *Nat Mater* 2005;4:435-46.
 56. Chandan HR, Schiffman JD, Balakrishna RG. Quantum dots as fluorescent probes: Synthesis, surface chemistry, energy transfer mechanisms, and applications. *Sens Actuators B: Chem* 2018;258:1191-214.
 57. Bruchez M Jr, Moronne M, Gin P, Weiss S, Alivisatos AP. Semiconductor Nanocrystals as Fluorescent Biological Labels. *Science* 1998;281:2013-2016.
 58. Chan WC, Nie S. Quantum Dot Bioconjugates for Ultrasensitive Nonisotopic Detection. *Science* 1998;281:2016-8.
 59. Jurado-Sánchez B, Escarpa A, Wang J. Lighting up micromotors with quantum dots for smart chemical sensing. *Chem Commun (Camb)* 2015;51:14088-91.
 60. Jurado-Sánchez B, Pacheco M, Rojo J, Escarpa A. Magnetocatalytic Graphene Quantum Dots Janus Micromotors for Bacterial Endotoxin Detection. *Angew Chem Int Ed Engl* 2017;56:6957-61.
 61. Luo PG, Sahu S, Yang ST, Sonkar SK, Wang J, Wang H, LeCroy GE, Cao L, Sun YP. Carbon "Quantum" Dots for Optical Bioimaging. *J Mater Chem B* 2013;1:2116-27.
 62. Li H, Kang Z, Liu Y, Lee ST. Carbon Nanodots: Synthesis, properties and applications. *J Mater Chem* 2012;22:24230-53.
 63. Molinero-Fernández Á, Moreno-Guzmán M, López MA, Escarpa A. Biosensing Strategy for Simultaneous and Accurate Quantitative Analysis of Mycotoxins in Food Samples Using Unmodified Graphene Micromotors. *Anal Chem* 2017;89:10850-7.
 64. Pacheco M, Jurado-Sánchez B, Escarpa A. Sensitive Monitoring of Enterobacterial Contamination of Food Using Self-Propelled Janus Microsensors. *Anal Chem* 2018;90:2912-7.
 65. Derfus AM, Chan WC, Bhatia SN. Probing the Cytotoxicity of Semiconductor Quantum Dots. *Nano Lett* 2004;4:11-8.
 66. Azhdarinia A, Ghosh P, Ghosh S, Wilganowski N, Sevick-Muraca EM. Dual-labeling strategies for nuclear and fluorescence molecular imaging: a review and analysis. *Mol Imaging Biol* 2012;14:261-76.
 67. Shao J, Xuan M, Zhang H, Lin X, Wu Z, He Q. Chemotaxis-Guided Hybrid Neutrophil Micromotors for Targeted Drug Transport. *Angew Chem Int Ed Engl* 2017;56:12935-9.
 68. Wang H, Potroz MG, Jackman JA, Khezri B, Maric T, Cho NJ, Pumera M. Bioinspired Spiky Micromotors Based on Sporopollenin Exine Capsules. *Adv Funct Mater* 2017;25:1702338.
 69. Su M, Liu M, Liu L, Sun Y, Li M, Wang D, Zhang H, Dong B. Shape-Controlled Fabrication of the Polymer-Based Micromotor Based on the Polydimethylsiloxane Template. *Langmuir* 2015;31:11914-20.
 70. Ikeuchi M, Isozaki K, Kyue K, Sunabe H, Shimada N, Sasago H, Ikuta K. Multifunctional optically driven microrobot for realtime 3D bio-manipulation and imaging. *Proceedings of the IEEE international conference on micro electro mechanical systems (MEMS)* 2011;41:29-32.
 71. Diao S, Blackburn JL, Hong G, Antaris AL, Chang J, Wu JZ, Zhang B, Cheng K, Kuo CJ, Dai H. Fluorescence Imaging In Vivo at Wavelengths beyond 1500 nm. *Angew Chem Int Ed Engl* 2015;54:14758-62.
 72. Corlu A, Choe R, Durduran T, Rosen MA, Schweiger M,

- Arridge SR, Schnall MD, Yodh AG. Three-dimensional in vivo fluorescence diffuse optical tomography of breast cancer in humans. *Opt Express* 2007;15:6696.
73. Kobayashi H, Hama Y, Koyama Y, Barrett T, Regino CA, Urano Y, Choyke PL. Simultaneous multicolor imaging of five different lymphatic basins using quantum dots. *Nano Lett* 2007;7:1711.
 74. Pimlott SL, Sutherland A. Molecular Tracers for the PET and SPECT Imaging of Disease. *Chem Soc Rev* 2011;40:149-62.
 75. Kim J, Lee N, Hyeon T. Recent Development of Nanoparticles for Molecular Imaging. *Philos Trans A Math Phys Eng Sci* 2017;375:20170022.
 76. Hedhli J, Czerwinski A, Schuelke MR, Ploska A, LaHood L, Czaplewska P, Mamer SB, Dobrucki IT, Sowinski P, Kalinowski L, Imoukhuede PI, Dobrucki LW. Synthesis, Chemical Characterization and Multiscale Biological Evaluation of a Dimeric-cRGD Peptide for Targeted Imaging of α V β 3 Integrin Activity. *Sci Rep* 2017;7:3185.
 77. Zhao Y, Pang B, Luehmann H, Detering L, Yang X, Sultan D, Harpstrite S, Sharma V, Cutler CS, Xia Y, Liu Y. Gold Nanoparticles Doped with ¹⁹⁹Au Atoms and Their Use for Targeted Cancer Imaging by SPECT. *Adv Healthc Mater* 2016;5:928-35.
 78. Cunha L, Horvath I, Ferreira S, Lemos J, Costa P, Vieira D, Veres DS, Szigeti K, Summavielle T, Máthé D, Metello LF. Preclinical imaging: an essential ally in modern biosciences. *Mol Diagn Ther* 2014;18:153-73.
 79. Tsang MK, Wong YT, Hao J. Cutting-Edge Nanomaterials for Advanced Multimodal Bioimaging Applications. *Small Methods* 2018;2:1700265.
 80. Qiu F, Zhang L, Peyer KE, Casarosa M, Frenco-Obregon A, Choi H, Nelson BJ. Noncytotoxic Artificial Bacterial Flagella Fabricated from Biocompatible ORMOCOMP and Iron Coating. *J Mater Chem B* 2014;2:357-62.
 81. Xu T, Yu J, Yan X, Choi H, Zhang L. Magnetic Actuation Based Motion Control for Microrobots: An Overview. *Micromachines* 2015;6:1346-64.
 82. Kim S, Lee S, Lee J, Nelson BJ, Zhang L, Choi H. Fabrication and Manipulation of Ciliary Microrobots with Non-reciprocal Magnetic Actuation. *Sci Rep* 2016;6:30713.
 83. Zhang L, Peyer KE, Nelson BJ. Artificial bacterial flagella for micromanipulation. *Lab Chip* 2010;10:2203-15.
 84. Zhang L, Abbott JJ, Dong LX, Kratochvil BE, Bell D, Nelson BJ. Artificial bacterial flagella: Fabrication and magnetic control. *Appl Phys Lett* 2009;94:064107.
 85. Li J, Sattayasamitsathit S, Dong R, Gao W, Tam R, Feng X, Ai S, Wang J. Template electrosynthesis of tailored-made helical nanoswimmers. *Nanoscale* 2014;6:9415-20.
 86. Yan X, Zhou Q, Yu J, Xu T, Deng Y, Tang T, Feng Q, Bian L, Zhang Y, Ferreira A, Zhang Li. Magnetite nanostructured porous hollow helical microswimmers for targeted delivery. *Adv Funct Mater* 2015;25:5333-42.
 87. Jin DD, Yu JF, Huang TY, Duan HL, Zhang L. Magnetic Micro-/Nanoscale Swimmers: Current Status and Potential Applications. *Chin Sci Bull* 2017;62:136-51.
 88. Qiu F, Fujita S, Mhanna R, Zhang L, Simona BR, Nelson BJ. Magnetic Helical Microswimmers Functionalized with Lipoplexes for Targeted Gene Delivery. *Adv Funct Mater* 2015;25:1666-71.
 89. Tottori S, Zhang L, Peyer KE, Nelson BJ. Assembly, Disassembly, and Anomalous Propulsion of Microscopic Helices. *Nano Lett* 2013;13:4263-8.
 90. Suter M, Zhang L, Siringil EC, Peters C, Luehmann T, Ergeneman O, Peyer KE, Nelson BJ, Hierold C. Superparamagnetic Microrobots: Fabrication by Two-Photon Polymerization and Biocompatibility. *Biomed Microdevices* 2013;15:997-1003.
 91. Peyer KE, Tottori S, Qiu F, Zhang L, Nelson BJ. Magnetic Helical Micromachines. *Chem Eur J* 2013;19:28-38.
 92. Zhang L, Petit T, Peyer K, Nelson BJ. Targeted Cargo Delivery Using a Rotating Nickel Nanowire. *Nanomedicine* 2012;8:1074-80.
 93. Tottori S, Zhang L, Qiu F, Krawczyk K, France-Obregon A, Nelson BJ. Magnetic Helical Micromachines: Fabrication, Swimming Control and Three-dimensional Cargo Transport. *Adv Mater* 2012;24:811-6.
 94. Petit T, Zhang L, Peyer KE, Kratochvil B, Nelson BJ. Selective Trapping and Manipulation of Microscale Objects Using Mobile Microvortices. *Nano Lett* 2012;12:156-60.
 95. Zhang L, Petit T, Lu Y, Kratochvil B, Peyer KE, Pei R, Lou J, Nelson BJ. Controlled Propulsion and Cargo Transport of Rotating Nickel Nanowires near a Patterned Solid Surface. *ACS Nano* 2010;4:6228-6234.
 96. Wang B, Liu Y, Zhang Y, Guo Z, Zhang H, Xin J, Zhang L. Bioinspired Superhydrophobic Fe₃O₄@Polydopamine@Ag Hybrid Nanoparticles for Liquid Marble and Oil Spill. *Adv Mater Interfaces* 2015;2:1500234.
 97. Chen XZ, Hoop M, Shamsudhin N, Huang TY, Ozkale B, Li Q, Siringil E, Mushtaq F, Tizio LD, Nelson BJ, Pane S. Hybrid Magnetoelectric Nanowires for Nanorobotic Applications: Fabrication, Magnetoelectric Coupling, and Magnetically Assisted In Vitro Targeted Drug Delivery. *Adv Mater* 2017;29:1605458.

98. Wang B, Chan KF, Yu JF, Wang QQ, Yang LD, Chiu PW, Zhang L. Reconfigurable swarms of ferromagnetic colloids for enhanced local hyperthermia. *Adv Funct Mater* 2018;28:1705701.
99. Medina-Sánchez M, Schmidt OG. Medical microbots need better imaging and control. *Nature* 2017;545:406-8.
100. Faivre D, Schuler D. Magnetotactic bacteria and magnetosomes. *Chem Rev* 2008;108:4875-98.
101. Benoit MR, Mayer D, Barak Y, Chen IY, Hu W, Cheng Z, Wang SX, Spielman DM, Gambhir SS, Matin A. Visualizing implanted tumors in mice with magnetic resonance imaging using magnetotactic bacteria. *Clin Cancer Res* 2009;15:5170-7.
102. Martel S, Felfoul O, Mahmood M. BioRob 2008. 2nd International Conference on Biomedical Robotics and Biomechatronics (IEEE RAS & EMBS); IEEE: Washington, D.C., 2008;264.
103. Martel S, Mohammadi M, Felfoul O, Lu Z, Pouponneau P. Flagellated magnetotactic bacteria as controlled MRI-trackable propulsion and steering systems for medical nanorobots operating in the human microvasculature. *Int J Rob Res* 2009;28:571-82.
104. Martel S, Felfoul O, Mathieu JB, Chanu A, Tamaz S, Mohammadi M, Mankiewicz M, Tabatabaei N. MRI-based nanorobotic platform for the control of magnetic nanoparticles and flagellated bacteria for target interventions in human capillaries. *Int J Rob Res* 2009;28:1169-82.
105. Felfoul O, Mohammadi M, Gaboury L, Martel S. Tumor Targeting by Computer Controlled Guidance of Magnetotactic Bacteria Acting Like Autonomous Microrobots. *Intelligent Robots and Systems International Conference (IROS) 2011*;25-30:1304-8.
106. Felfoul O, Martel S. Assessment of navigation control strategy for magnetotactic bacteria in microchannel: toward targeting solid tumors. *Biomed Microdevices* 2013;15:1015-24.
107. de Lanauze D, Felfoul O, Turcot JP, Mohammadi M, Martel S. Three-dimensional remote aggregation and steering of magnetotactic bacteria microrobots for drug delivery applications. *Int J Rob Res* 2014;33:359-74.
108. Chen Y, Kosmas P, Martel S. A feasibility study for microwave breast cancer detection using contrast-agent-loaded bacterial microbots. *Int J Antennas Propag* 2013;2013:309703.
109. Taherkhani S, Mohammadi M, Daoud J, Martel S, Tabrizian M. Covalent Binding of Nanoliposomes to the Surface of Magnetotactic Bacteria for the Synthesis of Self-Propelled Therapeutic Agents. *ACS Nano* 2014;8:5049-60.
110. Felfoul O, Mohammadi M, Taherhani S, Lanauze D, Xu YZ, Loghin D, Essa S, Jancik S, Houle D, Lafleur M, Gaboury L, Tabrizian M, Kaou N, Atkin M, Vuong T, Batist G, Beauchemin N, Radzioch D, Martel S. Magneto-aerotactic bacteria deliver drug-containing nanoliposomes to tumour hypoxic regions. *Nat. Nanotechnol* 2016;11:941-7.
111. Martel S, Tremblay CC, Ngakeng S, Langlois G. Controlled manipulation and actuation of micro-objects with magnetotactic bacteria. *Appl Phys Lett* 2006;89:257-681.
112. Behkam B, Sitti M. Modeling and testing of a biomimetic flagellar propulsion method for microscale biomedical swimming robots. *International Conference on Advanced Intelligent Mechanotronics Conference, 2005*;37-42.
113. Sanchez A, Magdanz A, Schmidt OG, Misra S. Magnetic control of self-propelled microjets under ultrasound image guidance. *5th IEEE RAS & EMBS International Conference on Biomedical Robotics and Biomechatronics (BioRob), 2014*;169-74.
114. Olson ES, Orozco J, Wu Z, Malone CD, Yi B, Gao W, Eghtedari M, Wang J, Mattrey RF. Toward in vivo detection of hydrogen peroxide with ultrasound molecular imaging. *Biomaterials* 2013;34:8918-24.
115. Khalil ISM, Ferreira P, Eleuterio R, Korte CL, Misra S. Magnetic-based closed-loop control of paramagnetic microparticles using ultrasound feedback. *IEEE International Conference on Robotics & Automation (ICRA) 2014*;3807-12.
116. Scheggi S, Chandrasekar KKT, Yoon C, Sawaryn B, Steeg G, Gracias DH, Misra S. Magnetic motion control and planning of untethered soft grippers using ultrasound image feedback. *2017 IEEE International Conference on Robotics and Automation (ICRA) 2017*;6156-61.
117. Yu J, Jin D, Zhang L. Mobile paramagnetic nanoparticle-based vortex for targeted cargo delivery in fluid. *2017 IEEE International Conference on Robotics and Automation (ICRA) 2017*;6594-9.
118. Yu J, Xu T, Lu Z, Vong C, Zhang L. On-demand Disassembly of Paramagnetic Nanoparticle Chains for Microrobotic Cargo Delivery. *IEEE Transactions on Robotics* 2017;33:1213-5.

Cite this article as: Wang B, Zhang Y, Zhang L. Recent progress on micro- and nano-robots: towards *in vivo* tracking and localization. *Quant Imaging Med Surg* 2018;8(5):461-479. doi: 10.21037/qims.2018.06.07